



Synthesis and characterization of fluorine doped tin oxide nanoparticle: An efficient catalyst for the preparation of 14-aryl-14H dibenzo [a,j]xanthene under free organic solvents conditions

Awad¹. Ahmed*, M. M. Eladl, W. S. Abo El-Yazeed

Chemistry Department, Faculty of Science, Mansoura University, Mansoura, Egypt

*Corresponding author: Chemistry Department, Faculty of Science, Mansoura University, Mansoura, Egypt. Tel.: +220502390551; fax: +220502246104. E-mail address: awahmed@mans.edu.eg (A.I. Ahmed)

Received: 18/1/2020
Accepted: 17/2/2020

Abstract: Stannic oxide SnO₂ nanoparticles were tailored using sol-gel approach, in which stannic chloride pentahydrate SnCl₄.5H₂O utilized as an inexpensive starting material. The obtained gel is dried then calcined at 450°C to form tetragonal SnO₂ structure (6.0 - 8.2 nm). The obtained powders are doped with different loading 10-55 wt. % of HF as a source of fluoride ion, followed by calcination at 200, 300 and 400°C. The surface acidity is examined for the fabricated samples with nonaqueous potentiometric titration versus n-butyl amine in acetonitrile. Surface acidity measurement results indicate that 45F-Sn contains the strongest acid sites. The calcination temperature 200°C is the ideal appropriate temperature for calcination at that the overall surfaces acidity and the acid strength reach to their maximum values. The catalytic efficiency was examined via solvent-free synthesis of 14-aryl-14H dibenzo [a,j] xanthene. 45F-Sn calcined at 200°C shows the highest catalytic activity and gives an excellent yield about 95.63%.

keywords: Tin oxide, Hydrofluoric acid, Nanoparticles, Surface acidity, Xanthenes.

1 Introduction

It is extensively recognized that there is an upward tendency for using friendly environmental approaches in chemical industries. This tendency headed for what has become defined as 'Green Chemistry'. Heterogeneous nanocatalysts considered an ideal choice for supporting the aspect of green chemistry represented in preparation of acidic solid catalysts for reasons such as pure products, no corrosion happening, no emulsion formation, and easier catalyst separation^[1]. The most significant part of catalysis applied in all fields of chemical industries is using solid acid catalysts. Broad categories of liquid phase industrial synthesis require using of inorganic or mineral acids. The main certain types of the reactions which are imperative in this situation are Friedel-Crafts acylations, alkylations and sulfonylations, aromatic isomerisations, nitrations, halogenations and oligomerisations. These reactions are commonly promoted by Lewis acids, for instance AlCl₃ and BF₃; and by mineral acids such as HF, HCl and H₂SO₄. However, using like these liquid catalysts have

complications associated with separation from product mixture, considered wastage, cost of process fitting and maintenance where these chemicals are risky in transferring, it is corrosive materials and could be destructive the plant, hence the need to find alternative catalyzed synthetic routes to eliminate such troubles. This could be reached with utilizing heterogeneous solid acid catalysts that are renewable materials, more stable and active at adequate temperatures^[2]. Solid acid catalysts possess the further advantages that the type of the active sites is recognized and may be defined by the existence of surface protons creating Brønsted acidity or coordinately unsaturated cations cores, i.e. Lewis acid sites^[3]. It is commonly identified that the applications of solid catalysts in industries are established on the base of their surface acidity, therefore, most of their catalytic properties associated with their acidity^[4]. Metal oxides symbolize the imperative category of materials which has intense applications in the area of catalysis as heterogeneous solid catalysts owing

to their excellent acid-base and redox characteristic [5]. These materials used as active phases or as support substances. One of between several metal oxides, tin oxide (SnO₂) gets the attention of the scientific society because of its twofold valence and its capability to acquire several oxidation states [6]. SnO₂ is explored in numerous significant organic reactions as an effective heterogeneous catalyst, where it has the appreciable acidic, basic, oxidizing and reducing surface characteristics. Furthermore tin oxide has an exceptional properties and applications where it has many positive properties, for example, high electrical conductivity, low electrical resistance and large optical transparency in the visible region of the electromagnetic range [7]. Owing to these properties, SnO₂ has a broad range of very interesting applications such as solar cells [8], gas sensor [9], electrode for lithium batteries [10] and etc

Many studies have been reported on modified SnO₂ catalysts with another materials such as impregnated tin oxides with calcium for Babassu oil transesterification [11], antimony doped tin oxide [12], modified tin dioxide with iodine doped titanium dioxide for the photocatalytic degradation of ortho-chlorophenol under visible light irradiation [13], WO₃/SnO₂ catalysts for production of biodiesel [14], sulfated tin oxide for the preparation of coumarin [15], H₃PW₁₂O₄₀ supported on tin oxide for the preparation of coumarin [16], phosphomolybdic acid /SnO₂ as an efficient catalyst [2],.....etc. The suitable selection of the additives materials is very important in adjusting the surface characteristics of a catalyst.

The doping of SnO₂ can occur with donor elements as indium, antimony which substitute Sn (IV) sites [17, 18] or fluorine (F) that replaces the oxygen sites [19].

The doping of SnO₂ with fluorine results in reaching the highest electronic conductivity and IR reflectivity due to the identical ionic radii of F⁻ and O²⁻ in SnO₂ and acts as a donor in SnO_x:F [20]. Fluorine-doped SnO₂ catalysts are used in solar cells [21], gas sensors [22, 23], touch panels [24], substrates for electro-deposition [25] and light emitting diodes [26]. Different techniques such as chemical vapour deposition

[27], spray pyrolysis [28], RF-sputtering [29], pulsed laser deposition [22], sol-gel processes and [30] inkjet printing [31] have been employed to produce fluorine-doped tin oxide films.

Recently, the interest in the synthesis of aryl-14*H*-dibenzo[*a,j*]xanthene's is attracted more attention due to its pharmacological, therapeutic and spectroscopic properties. It has been reported as antiviral, bactericide and anti-inflammatory agents [32, 33, 34]. Furthermore, it's applied in industries as dyes, fluorescent materials for visualization of biomolecules, in laser technologies [35, 36, 37], photodynamic therapy [38] and antagonism of the paralyzing action of zoxazolamine [39]. Aryl-14*H*-dibenzo[*a,j*]xanthene's are synthesized from the condensation reaction of benzaldehyde with β-naphthol, this reaction is catalyzed by many Brønsted acid catalysts such as H₃PO₄ or HClO₄ at 0°C in acetic acid [40], H₂SO₄ [36], heteropolyacid [41], sulfamic acid [42], silica sulfuric acid [43], *p*-toluenesulfonic acid [44], methanesulfonic acid [45], AcOH/H₂SO₄ [36], cyanuric chloride [46], CoPy₂Cl₂ [47], LiBr [48], ruthenium chloride hydrate [49], Yb(OTf)₃ [50], Al(HSO₄)₃ [51], Sc[N(SO₂C₈F₁₇)₂]₃ [52], NaHSO₄ [53], silica chloride [54], P₂O₅ /Al₂O₃ [55], bismuth(III)chloride [56], silica supported perchloric acid [57] and ZrO(OTf)₂ [58].

In this work, tin oxide has been prepared using the sol-gel method as effective and low-cost pathway. The impact of fluorine as a dopant for enhancing the surface acidity of tin oxide is also considered. The catalytic activity of the fabricated catalysts is studied using a condensation reaction of benzaldehyde and β-naphthol for producing 14-aryl-14*H* dibenzo [a,j] xanthene.

2. Experimental

2.1. Preparation of SnO₂ and fluoride doped SnO₂

The tin oxide was prepared by sol-gel method. 10 g of SnCl₄.5H₂O (Sigma Aldrich) was dissolved in 50 ml ethanol (Alfa Aesar, 98% purity) with stirring for 15 min, followed by adding of NH₄OH (25 wt.% solution) dropwise until the formation of the white gel of Sn(OH)₄ (pH≈8.5). After vigorous stirring for 2 h, the white gel was filtered and washed several times with CH₃COONH₄ (2 wt.% solution) till eliminating all chloride ions (the absent of Cl⁻

ions was checked by 0.1N AgNO₃ solution). The obtained tin hydroxide gel was dried at 120 °C overnight then calcined at 450 °C for 3 h with a rate of 5.0 °C/min.

A series of catalysts with fluoride content 10, 25, 35, 45, and 55 wt.% was fabricated as follow : 3.0 g of SnO₂ was sonicated with 30 ml dist. H₂O and agitated for 30 min in a plastic beaker, then the suitable volume of 2M HF solution was mixed with the tin oxide suspension dropwise with stirring for 3 h. The product was aged at room temperature for 48 h, the resulting product was filtered and dried at 120 °C for 2 h, then calcined at 200 °C for 2 h with a rate 5.0 °C/min and 45 wt.% F-SnO₂ sample was calcined at 300 and 400 °C.

In designating the various samples F and Sn stand for fluoride and tin oxide, respectively. The numbers 10, 25, 35, 45, and 55 before F indicate the fluoride content. The roman numerals I, II and III after Sn indicate the calcination temperature of 200, 300 and 400 °C respectively. Thus, for example, 25F-Sn-II will indicate 25 wt.% fluoride loaded on SnO₂ and the sample calcined at 300 °C.

2.2. Catalyst characterization

The XRD patterns were examined using X-ray powder diffractometer (PW150 Philips) through the radiation of nickel-filtered Cu-K α ($\lambda = 1.540 \text{ \AA}$) at 2θ of 20 to 70 °, 40 kV and 30 mA. The calculation of the crystallite size (nm) was achieved by applying the Debye- Scherrer equation [59].

$$D = \frac{k\lambda}{\beta \cos \theta}$$

37.9 and 51.7°, which are assigned to (110), (101), (200), (211), and (310) crystallographic faces of SnO₂ (reference JCPDS cards no 41-1445). It can be seen that the SnO₂ obtained has a crystalline tetragonal cassiterite structure [27]. No diffraction lines belonged to tin fluoride structures were noticed in the sample patterns. This is may be due to the small size of fluoride particles or a good dispersion of the fluoride element on the surface as well as inside the pores of SnO₂ [20, 62-64]. In the current study, the intensity of the (200) plane improves with increasing the fluorine level up to 45 wt.% (45 F-Sn-I) and then depreciated with fluorine content up to 55 wt.% (55 F-Sn-I). It was

observed also that the peaks intensity decreases with increasing the fluoride content while the full-width half-maximum (FWHM) increases which indicate that both the growth and the orientation depend on the crystal lattice strain and so the crystallinity decreases. Due to the solubility limit of fluoride ions in SnO₂ lattice, the excess of fluoride ions occupies the interstitial sites in tin oxide lattice [63] which may be lead to the point defects and the alteration in stoichiometric as a result of the charge difference. This is, in turn, increases the disorder of the lattice and decreases the contact of particles due to high fluoride electro-negativity [64], and thus, decreases the crystalline size of SnO₂. Kumar et al. [65] attributed the decreasing in crystallite size to the incorporation of fluoride ions in oxygen sites in SnO₂ lattice whereas the very high electro-negativity of fluoride causes a reduction in the nuclei size and grain size. Fig. 2 illustrates the influence of different calcination temperatures on the crystallinity of 45 F-Sn sample. The patterns display a reduction in the intensities with rising the calcination temperatures, therefore the samples calcined at 300 and 400 °C showing high crystallite size than the samples calcined at 200 °C. This may be due to the evaporation of some F⁻ ions from the surface of the catalyst by increasing the calcination temperatures SnO₂ [15].

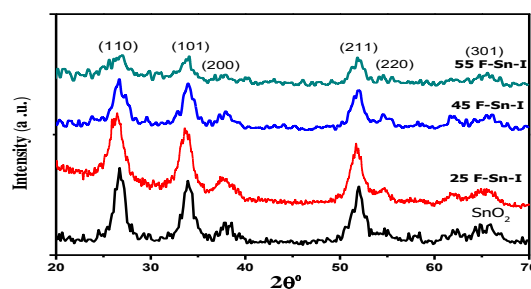


Fig. 1: XRD patterns of F-Sn samples.

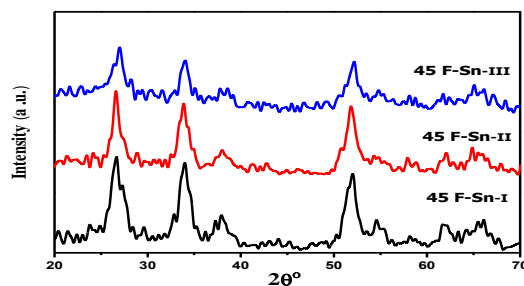


Fig. 2: XRD patterns of 45 F-Sn sample calcined at different temperatures.

The average crystallite size that determined for the most intense diffraction line (110) using Scherrer's equation ^[66] are recorded in Table.1. The results displayed that increasing the loading of fluoride up to 45 wt. % causes a decrease in the SnO₂ crystallinity while a further increase of fluoride to 55 wt.% causes the crystallite size to be increased which may be ascribed to the aggregation of fluoride clusters on tin oxide surface. Meanwhile, there is a gradual increase in the crystallite size of 45 F-Sn with increasing the calcination temperatures from 200 to 400 °C as a result of the evaporation of some F⁻ ions by increasing the thermal energy, in all cases the average crystallite size of treated SnO₂ is still less than the pure one. The nominal fluorine concentration in the starting solution and the final concentration obtained from XPS results are listed in Table 2. It is noticed that the F content in the solid catalysts is less than that was taken in the starting solution. For attainment the optimum surface acidity hence activity of the catalysts, the starting with high concentration of F ions in preparation is required ^[67, 68]. This is may be due to when the fluorine sources from the HF were poured into the suspended solution with tin oxide; gases were escaped or disappeared into the surroundings during the doping process ^[64, 67].

3.2. Surface Acidity Measurements

The strength of surface acidity and the overall acidic sites number are calculated by measuring the electrode potential (mV) against the regular increase in the concentration of the n-butylamine ^[69]. The initially electrode potential (Ei) values indicate the strength of the surface acid sites ^[16, 70]. Fig. 3 shows the titration curves for pure tin oxide and F- doped tin oxide calcined at 200 °C, the acid sites total number and the (Ei) values of the prepared samples are collected in Table 1. It can be observed that the surface acidity and the number of acidic sites are increased by the addition of F⁻ to tin oxide. The initial electrode potential (Ei) of pure tin oxide (calcined at 450 °C) is equal to 94.3 mV, this value is increased gradually by increasing F⁻ loading to reach its maximum value for the sample 45 F-Sn-I at which (Ei=450.0 mV). 45 F-Sn-I catalyst has the largest overall number of acid sites and highest acidic strength. These results can be

taken as an indication on the role of F⁻ for the enhancement of the surface acidity and may be due to good dispersion of the fluoride ions on the surface and inside the pores of SnO₂ and/or the replacement of oxygen of tin oxide by F⁻ to form SnO_{2-x}F_x structure. These processes strengthen the Brønsted acidity that in role resulted in increasing the acidity and the acid strength ^[71]. The surface acidity is decreased by the increase in the F⁻ content above 45wt.% which may be as a result of the formation of more than one layer from the fluoride ions on the surface of the tin oxide. Fig. 4 evinces the influence of the calcination temperature on the surface acidity behavior of the 45 F-Sn catalyst. The initial electrode potential (Ei) and the overall number of acid sites were found to decrease, Table 1, with rising the calcination temperature up to 300 and 400 °C. The drop in surface acidity with the rise of calcination temperature may be owing to the liberation of F⁻ from SnO₂ surface ^[65]. This confirms that the distribution of F⁻ on the surface and in the structure of SnO₂ was responsible for enhancement the acidity, and calcination temperature 200 °C is the optimum calcination temperature for the catalyst uses. Parida et al. ^[72] found that the addition of F⁻ ions to SO₄²⁻/TiO₂-SiO₂ increases the acid strength because of the inductive effect of S=O and gem-fluoride ions.

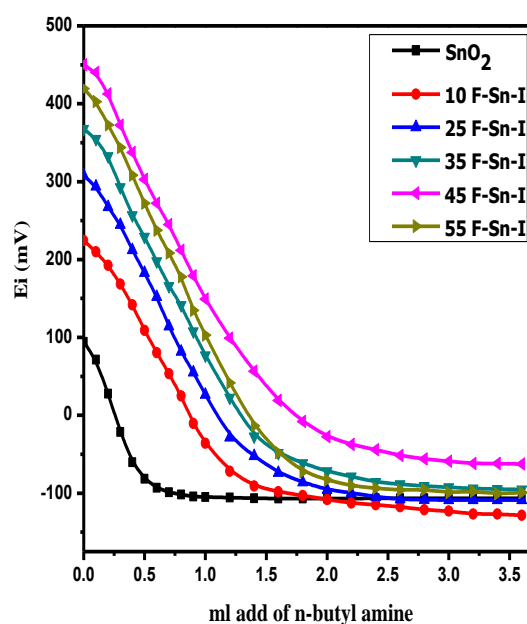


Fig. 3: Potentiometric titration of n-butylamine in acetonitrile for F-Sn samples.

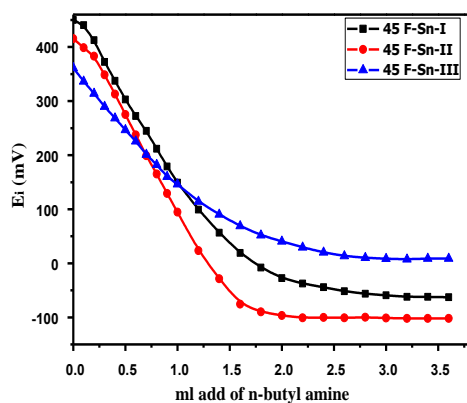


Fig. 4: Potentiometric titration of n-butylamine in acetonitrile for 45 F-Sn samples at different calcination temperatures.

The type of acidic sites on the catalysts surface is measured by the adsorption of pyridine. The pyridine adsorbed over the Brønsted acid sites as pyridinium cation and as a coordinated molecule on the Lewis acid site. The IR spectrums of adsorbed pyridine on the fluoride doped SnO₂ catalysts calcined at 200 °C for 10 F-Sn, 25 F-Sn, 35 F-Sn, 55 F-Sn and for 45 F-Sn sample calcined at 200, 300 and 400 °C are illustrated in Fig. 5 and Fig. 6, respectively. The spectra show two bands at around 1630 cm⁻¹ and 1440 cm⁻¹ that assigned for the Brønsted and Lewis acid sites, respectively [73]. The ratio of Brønsted (B) and Lewis (L) acid sites was calculated from the integrated area of the bands at 1630 cm⁻¹ and 1440 cm⁻¹ [74], and the results are recorded in Table 1. As shown in Fig.5, the band intensity assigned to Brønsted acidic sites is greater than that assigned to Lewis acidic sites. The relative intensities and the integrated areas of the bands which belong to Brønsted sites are increased regularly with an increase in F⁻ content till 45wt.%, while that which belong to Lewis sites are remaining semi-constant. These results indicated that the incorporation of F⁻ to the precalcined SnO₂ samples lead to strength the free acidic protons on the tin oxide surface and consequently, the Brønsted acid sites increases as a response for surface acidity increasing [71]. Both Brønsted and Lewis acid sites are present in the fluoride doped SnO₂ catalysts and are varied with the F⁻ content and the catalyst 45 F-Sn-I has the highest Brønsted acid sites and B/L ratio. Fig. 6 illustrates the influence of the variation in the calcination temperatures on the

quantity of pyridine adsorbed on the 45 F-Sn sample. As seen, decreasing the intensity of the band assigned to Brønsted acid sites with rising the calcination temperature as a result of the removal of some F⁻ from the SnO₂ structure which in turn weaken some hydrogen proton on SnO₂ surface and consequently Brønsted acid sites and B/L ratio [15].

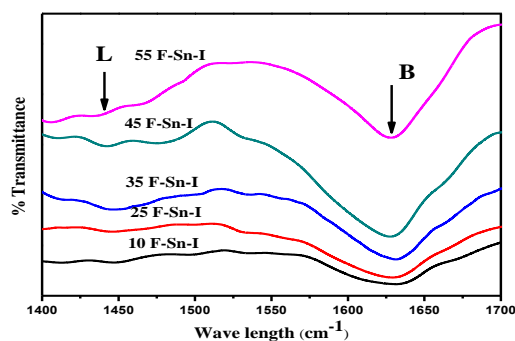


Fig. 5: FTIR spectra of pyridine adsorbed on F-Sn samples.

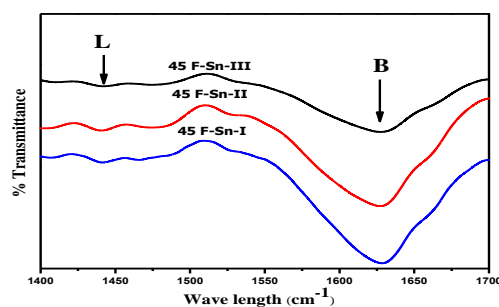


Fig. 6: FTIR spectra of pyridine adsorbed on F-Sn samples.

3.3. Catalytic activity

The condensation reaction of benzaldehyde and 2-naphthol was carried out using the investigated catalysts at 120°C under free solvent condition to get 14-Aryl-14-H-dibenzo [a,j]xanthene. The reaction carried out in absence of catalysts and no yield has been detected.

The reaction was carried out over 0.1 g of pure and modified tin oxide with fluoride at 120°C for two hours to detect the effect of fluoride loading on the activity of the catalysts. The modified tin oxide with fluoride show increasing in its activity whereas the pure tin oxide exhibits a low yield percentage for desired product (36.2%) While that the modified one show a progressive increasing in the catalytic activity with fluoride loading increases to give a maximum activity (95.63%)

at 45%wt. F⁻ then decrease to 84.1% with further fluoride content (Fig.7 and Table 1. It is known that the catalytic activity of the catalyst largely affected with its surface acidity. Fig. 8 and Fig. 9 demonstrate the influence of fluoride content on the acid property of the catalysts where the initial electrode potential and number of acid sites increase regularly with increasing the fluoride content till reach to maximum at 45%wt. F⁻ then decrease with increasing the fluoride content which conducted with the yield percentage for formation of the desired product.

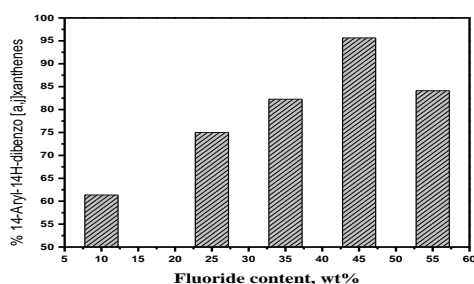


Fig. 7: Effect of fluoride content, wt.%, on 14-aryl-14-H-dibenzo [a,j]xanthenes synthesis.

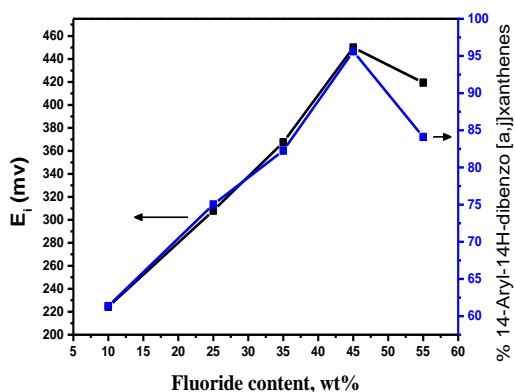


Fig. 8: Effect of F⁻ content, wt.% on acid strength and % 14-aryl-14-H-dibenzo [a,j] xanthenes.

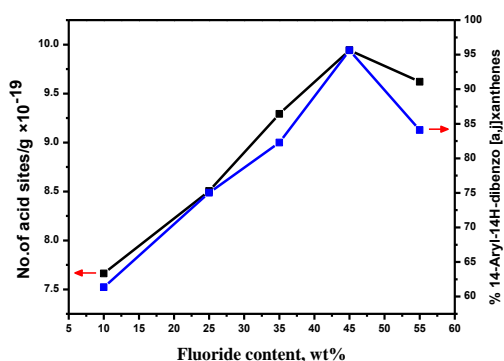


Fig. 9: Effect of F⁻ content, wt.% on total number of acid sites and % 14-Aryl-14-H-dibenzo [a,j] xanthenes.

The reaction was proceed with 0.1 g of 45F-Sn-I as a catalysts with different benzaldehyde: β-naphthol molar ratio to determine the influence of molar ratio on the formation of 14-aryl-14-H-dibenzo [a,j]xanthenes. As illustrated in Fig. 10, the yield percentage of the desired product growing from 69.2% to 95.63% with the rising molar ratio of benzaldehyde: 2-naphthol from 1:1 to 1:1:2 respectively, a significant decline in the yield percentage of 14-aryl-14-H-dibenzo [a,j]xanthenes to 85.6% was noticed with further increasing in molar ratio to 1:3. The lessening in catalytic activity may be elucidated on the basis of the fact that the rise in the benzaldehyde concentration impedes the reaction by obstructive the active sites on the catalyst surface.

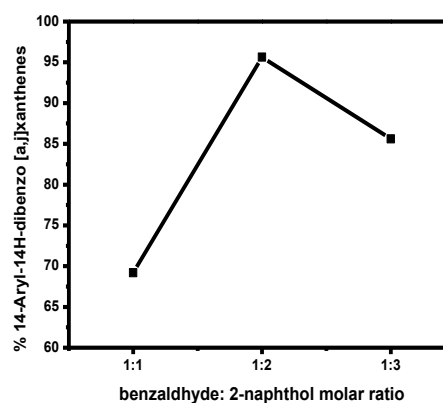


Fig. (10): Effect of molar ratio of benzaldehyde: β-naphthol on the synthesis of 14-aryl-14-H-dibenzo [a,j]xanthenes in the presence of (45F-Sn-I) as a catalyst.

The effect of calcination temperature for 45 F-Sn-I sample calcined at 200, 300 and 400°C on the 14-Aryl-14-H-dibenzo [a,j]xanthenes formation was studied. From Fig. 11, Fig. 12 and Table. 1, we can see the yield percentage decrease with increasing the calcination temperature, whereas 45F-Sn calcined at 200°C give highest yield (95.63%) and rising the calcination temperature to 300 and 400°C led to decreasing the

yield to 88.32 and 77.87% respectively. As presented in Fig. 11 and Fig. 12, the catalytic activity and hence yield percentage of the desired product are closely related to the acid strength and the overall number of acid sites, which in turn affected with the calcination temperature of the catalyst.

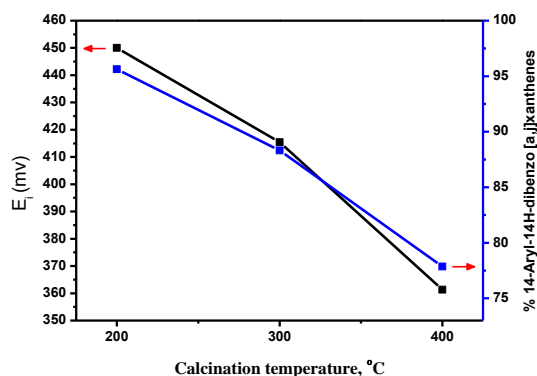


Fig. 11: The effect of different calcination temperatures on acid strength and formation of 14-aryl-14-H-dibenzo [a,j]xanthene

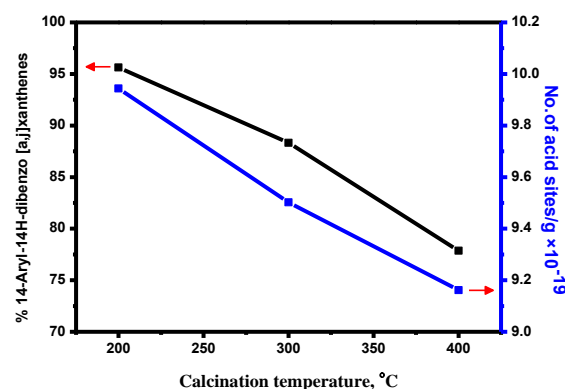


Fig. 12: The effect of different calcination temperatures on the total number of acid sites and formation of 14-aryl-14-H-dibenzo [a,j]xanthene

Table 1: Surface acidity, catalytic activity and crystallite size of F-Sn catalysts
Table 2: Nominal and final composition of the F-Sn catalysts.

Sample	E_i (mV)	No. of acid sites/g $\times 10^{-19}$	Conversion percentage of 14-Aryl-14-H-dibenzo [a,j]xanthene	B/L	Crystallite size (nm)
SnO ₂	94.3	2.9617	36.2	--	8.2
10 F-Sn-I	224.35	7.6628	61.35	4.4	--
25 F-Sn-I	308	8.5038	75.02	4.66	7.0
35 F-Sn-I	367.5	9.2913	82.27	4.83	--
45 F-Sn-I	450	9.9438	95.63	10.96	6.2
55 F-Sn-I	419.4	9.6197	84.1	8.18	7.3
45 F-Sn-II	415.4	9.5023	88.32	9.2	6.9
45 F-Sn-III	361.3	9.1615	77.87	6.28	7.6

Table 2: Nominal and final composition of the F-Sn catalysts.

Nominal F (wt%)	F(wt%) from XPS data
10	1.9
25	5.2
35	7.1
45	9.2
55	11.9

4. Conclusion:

F ion with different content (10-55 wt,%) doped SnO₂ nanopowders have been purposefully fabricated at different calcination temperatures based on sol gel route. The XRD studies of the prepared catalysts showed the tetragonal cassiterite structure of SnO₂ with crystallite size in nanometric range (6.0- 8.2 nm). Surface acidity was measured using potentiometric titration and adsorbed pyridine. The results indicated that the doping of SnO₂ with fluoride increases the Brønsted acid sites strength which in role increases the B/L ratio. The catalytic activity of the catalysts was examined with synthesis of 14-aryl-14H dibenzo [a,j] xanthene. The results indicated

that the catalytic activity of the catalysts is closely related to the acid strength and B/L ratio which in turn related to the fluoride content in the catalysts. Increasing the calcination temperature from 200 to 300 and 400 °C resulted in the removal of F⁻ from the surface and the structure of SnO₂ which decrease the Brønsted acidity and the catalytic activity. The results of characterization techniques revealed that the catalyst contain 45%wt. of fluoride and calcined at 200°C is the optimum one.

4. References

- 1 E. Tabrizian, A. Amoozadeh, S. Rahmani, RSC Adv., 6 (2016) 21854-21864.
- 2 S. M. Hassan, A. A. Ibrahim, S. A. El-Hakam, M. A. Mannaa, (2013) *Int. j. modern chem.*, **4(2)**, 104-116.
- 3 N. Liu, X. Pu, X. Wang, L. Shim, (2014) *J. Indus. Eng. Chem.*, **20** 2848-2857
- 4 G. Busca, Progress in Mater. Sci., **104** (2019) 215-249.
- 5 R. Varala, V. Narayana, S. R. Kulakarni,

- M. Khan, A. Alwarthan, S. F. Adil, (2016) *Arab. J. Chem.* **9** 550–573.
- 6 M. Batzill, U. Diebold, *Prog. (2005) Surf. Sci.*, **79** 47-154.
- 7 B. V. Mistry, D. K. Avasthi, U. S. Joshi, (2016) *Appl. Phys. A*, **122** 1024.
- 8 S. Ferrere, A. Zaban, B.A. Gregg, (1997) *J. Phys. Chem. B*, **101** 4490-4493.
- 9 A. R. Phani, S. Manorama, V. J. Rao, (2000) *J. Phys. Chem. Solids* 61 985.
- 10 A. Yu, R. Frech, (2002) *J. Power Sources*, **104** 97.
- 11 J. L. Solis, L. Alejo, Y. Kiros, (2016) *J. Environ. Chem. Eng.*, **4** 4870–4877.
- 12 H. Sun, X. Liu, B. Liu, Z. Yin, (2016) *Mater. Res. Bull.*, **83** 354–359.
- 13 Z. He, C. Wang, H. Wang, F. Hong, X. Xu, J. Chen, S. Song, (2011) *J. Hazard. Mater.*, **189** 595–602.
- 14 W. Xie, T. Wang, (2013) *Fuel Process. Technol.*, **109** 150-155.
- 15 A. I. Ahmed, S. A. El-Hakam, A. S. Khder, W. S. Abo El-Yazeed, (2013) *J. Mol. Catal. A-Chem.*, **366** 99– 108.
- 16 A. I. Ahmed, S. A. El-Hakam, M. A. Abd Elghany, W. S. Abo El-Yazeed(2011), *Appl. Catal. A-Gen.*, **407** 40– 48.
- 17 S. S. Lekshmy, K. Joy, (2014) *J. Mater. Sci. - Mater. Electron.* **25** 1664–1672.
- 18 E. Elangovan, K. Ramesh, K. Ramamurthi, (2004) *Solid State Commun.* **130** 523–527.
- 19 A. V. Moholkar, S. M. Pawar, K.Y. Rajpure, C.H. Bhosale, (2009) *J. H. Kim, Appl. Surf. Sci.* **255** 9358–9364.
- 20 M. Thirumoorthi, J. T. J. Prakash, (2016) *Superlattices Microstruct.* **89** 378-389.
- 21 I. Y. Y. Bu, *Ceram. (2014) Int.* **40** 417–422.
- 22 H. Kim, R.C.Y. Auyeung, A. Piqué, (2008) *Thin Solid Films*, **516** 5052–5056.
- 23 C. H. Han, D.U. Hong, J. Gwak, S.D. Han, Korean(2007) *J. Chem. Eng.* **24** 927–931.
- 24 S. F. Tseng, W. T. Hsiao, K. C. Huang, D. Chiang, (2011) *Appl. Surf. Sci.* **257** 8813–8819.
- 25 M. R. Khelladi, L. Mentar, M. Boubatra, A. Azizi, A. Kahoul, (2010) *Mater. Chem. Phys.* **122** 449–453.
- 26 A. G. Macedo, E. A. de Vasconcelos, R. Valaski, F. Muchenski, E. F. da Silva Jr., A. F. da Silva, L.S. Roman, (2008) *Thin Solid Films*, **517** 870–873.
- 27 Q. Gao, H. Jiang, C. Li, Y. Mab, X. Li, Z. Ren, Y. Liu, C. Song, G. Han, (2013) *J. Alloys Compd.* **574** 427–431.
- 28 A. Benhaoua, A. Rahal, B. Benhaoua, M. Jlassi, (2014) *Superlattices Microstruct.* **70** 61–69.
- 29 M. Acosta, Rocío Acosta Méndez, I. Riech, Manuel Rodríguez-Pérez, Geonel Rodríguez-Gattorno, (2019) *Superlattices Microstruct.* **127** 123-127.
- 30 P. K. Biwas, L. Dua, A. De, T. Chaudhuri, (2006) *Mater. Sci.* **24** 367–374.
- 31 A. J. S. Ahammad, P. R. Pal, S. S. Shah, T. Islam, M. M. Hasan, M. A. A. Qasem, N. Odhikari, S. Sarker, D. MinKim, M. Abdul Aziz, (2019) *J. Electroanal. Chem.* **832** 38-379.
- 32 J. P. Bacci, A. M. Kearney, D. L. van Vranken, (2005) *J. Org. Chem.*, **70** 9051–9053.
- 33 C. G. Knight, T. Stephenes, (1989) *J. Biochem.*, **258** 683–687.
- 34 K. Chibale, M. R. Visser, D. van Schalkwyk, P. J. Smith, A. Saravanamuthu, A. H. Fairlamb, (2003) *Tetrahedron*, **59** 2289–2296.
- 35 K. Singh, D. Arora, S. Singh, (2006) *Tetrahedron Lett.*, **47** 4205–4207.
- 36 R. J. Sarma, J. B. Baruah, (2005) *Dyes Pigments*, **64** 91–92.
- 37 S. K. Ko, C. F. Yao, (2006) *Tetrahedron Letters*, **47** 8827–8829.
- 38 A. Banerjee, A. K. Mukherjee, (1981) *Stain Technol.*, **56** 83–85.
- 39 G. Saint-Ruf, H. T. Hieu, J. P. Poupelin, (1975) *Naturwissenschaften*, **62** 584.
- 40 S. B. Patil, R. P. Bhat, S. D. Samant, (2006) *Synth. commun.*, **36** 2163.
- 41 M. Seyyedhamzeh, A. Bazgir, (2007) *Appl. Catal. A: General*, **323** 242.
- 42 D. Liu, Y. Yu, W. Shi, Ch. Liu, G. Luo, (2007) *Preparative Biochem. Biotech.*, **37** 77.
- 43 H. R. Shaterian, M. Ghashang, A. Hassankhani, (2008) *Dyes and Pigments* **76** 564.
- 44 B. Rajitha, B. Sunil Kumar, Y. Thirupathi Reddy, P. Narsimha Reddy, N. (2005) Sreenivasulu, *Tetrahedron Lett.*, **46** 8691–

- 8693.
- 45 A. Khoramabadi-zad, Z. Kazemi, H. A. Rudbari, (2002) *J. Korean Chem. Soc.*, **46** 541.
- 46 M. A. Bigdeli, M. M. Heravi, G. H. Mahdavinia, (2007) *Catal. Commun.*, **8** 1595.
- 47 J. V. Madhav, B. S. Kaurm, B. Rajitha, (2008) *Arkivoc* ii 204.
- 48 A. Saini, S. Kumar, J. S. Sandhu, Synlett, (2006) 20061928–1932.
- 49 K. Tabatabaeian, A. R. Khorshidi, M. Mamaghani, A. Dadashi, (2011) *Synth. Commun.*, **41** 1427.
- 50 W. Su, D. Yang, C. Jin, B. Zhang, (2008) *Tetrahedron Lett.*, **49** 3391.
- 51 H. R. Shaterian, M. Ghashang, N. Mir, *Arkivoc* xv (2007) 1.
- 52 M. Hong, C. Cai, (2009). *J. Fluorine Chem.*, 130 989.
- 53 Z. K. Jaber, M. M. Hashemi, (2008) *Monatsh. Chem.*, **139** 605.
- 54 L. Wu, C. Yang, L. Yang, L. Yang, (2010) *Phosphorus, Sulfur, and Silicon*, 185 903.
- 55 A. Zarei, A. R. Hajipour, L. Khazdooz, *Dyes and Pigments*, **85** (2010) 133.
- 56 E. Soleimani, M. M. Khodaei, A. Taheri Kal Koshvandi, (2011) *Chin. Chem. Lett.*, **22** 927.
- 57 L. Q. Wu, Y. F. Wu, C. G. Yang, L. M. Yang, L. J. Yang, (2010) *J. Braz. Chem. Soc.*, **221** 941.
- 58 M. Moghadam, S. Tangestaninejad, V. Mirkhani, I. Mohammadpoor-Baltork, H. R. Tavakoli, (2011) *Chin. Chem. Lett.*, **22** 9.
- 59 W.S. Abo El-Yazeed, A. I. Ahmed, (2019) *Inorg. Chem. Commun.* **105** 102-111.
- 60 A. I. Ahmed, S. A. El-Hakam, S. E. Samra, A. A. EL-Khouly, A. S. Khder, (2008) *Colloids Surf., A* **317** 62 – 70.
- 61 H. Matsushashi, H. Motoi, K. Arata, (1994) *Catal. Lett.* 26 325- 328.
- 62 A. H. O. Alkhayatt, S. K. Hussian(2015), *Mater. Lett.* 155 109–113.
- 63 B. Zhang, Y. Tian, J. X. Zhang, W. Cai, (2011) *Mater. Sci.* **46** 1884–1889.
- 64 W. Z. Samad, M. Gotob, H. Kanda, Wahyudionob, N. Nordina, K. H. Liew, M. A. Yarmo, M. R. Yusop, (2017) *J. Supercrit. Fluids*, **120** 366–378.
- 65 A. Kumar, S. K. Swami, V. Dutta, (2014) *J. Alloys Compd.* **588** 546–550.
- 66 S. M. Hassan, A. I. Ahmed, M. A. Mannaa, (2018)*Ceram. Int.* **44** 6201-6211.
- 67 H. Cachet, A. Gamard, G. Campet, B. Jousseau, T. Toupance, (2001) *Thin Solid Films*, **388** 41-49.
- 68 A.N. Banerjee, S. Kundoo, P. Saha, K.K. Chattopadhyay, (2003) *J. Sol-Gel Sci. Technol.* **28** 105–110.
- 69 M. Langpape, J. M. M. Millet, U. S. Ozkan, M. Boudeul, (1999) *J. Catal.* **181** 80-90.
- 70 T. Klimova, E. Carmona, J. Ramirez, (1998) *J. Mater. Sci.* **33** 1981-1990.
- 71 B. R. Jermy, A. Pandurangan, (2008) *Catal. Commun.* **9** 577–583.
- 72 S. K. Samantaray, K. Parida, (2004) *J. Mater. Sci.* **39** 3549 – 3562.
- 73 L. K. Noda, R. M. d. Almeida, L. F. D. Probst, N. S. Goncalves, (2005) *J. Mol. Catal. A: Chem.* **225**39-46.
- 74 B. R. Jermy, A. Pandurangan, (2005) *J. Mol. Catal. A: Chem.* **237** 146-154.